JOURNAL OF GUIDANCE, CONTROL, AND DYNAMICS
Vol. 30, No. 4, July–August 2007

Integrated Sliding Mode Autopilot-Guidance for Dual-Control Missiles

Moshe Idan* and Tal Shima†
Technion–Israel Institute of Technology, 32000 Haifa, Israel
and
Oded M. Golan‡
RAFAEL, Ministry of Defense, 31021 Haifa, Israel

DOI: 10.2514/1.24953

An integrated autopilot and guidance algorithm is developed, using the sliding mode control approach, for a missile with forward and aft control surfaces. The integrated controller can account simultaneously for the guidance and autopilot requirements using the additional degree of freedom offered by the dual-control configuration. Based on guidance considerations, the zero-effort miss, encountered in differential games guidance solutions, is used as one of the sliding variables in the proposed control scheme. Selection of the second surface, required due to the dual-control configuration, is based on autopilot design considerations. Restraining the system to the zero-effort miss surface guarantees zero-miss distance, whereas remaining on the second surface provides a damped response. The performance of the integrated dual controller is evaluated using a two-dimensional nonlinear simulation of the missile lateral dynamics and relative kinematics. The simulation results validate the design approach of using zero-effort miss and the flight-control based sliding surfaces to attain high-accuracy interception in engagements against highly maneuvering targets.

Nomenclature

A, B, C, G	=	state space model matrices
a	=	acceleration
$f_{(\cdot)}(\cdot)$	=	missile nonlinear aerodynamics function
$\boldsymbol{f}, \boldsymbol{g}$	=	vector functions
H	=	matrix used to determine the sliding mode control signal
I	=	moment of inertia
$\mathcal{L}$	=	Lyapunov function candidate
L	=	lift force
$L_{(\cdot)}$	=	lift force derivative
$\mathcal{M}$	=	sliding mode control uncertainty controller parameter matrix
M	=	pitch moment
$M_{(\cdot)}$	=	pitch moment derivative
m	=	mass
q	=	pitch rate
r	=	range
t, t_{go}	=	time, time-to-go
U_m	=	saturation limit
V	=	speed
X–M–Z	=	body reference frames
X–O–Z	=	inertial reference frame
$\boldsymbol{x}$	=	state vector
Z	=	zero-effort miss
z	=	target-missile relative displacement normal to the initial line of sight
α	=	angle of attack
γ	=	flight path angle
$\Delta\phi$	=	maneuver phase
ΔT	=	target maneuver period
$\Delta, \bar{\Delta}$	=	modeling errors and their bounds
δ	=	control surface deflection angle
$\boldsymbol{\delta}$	=	vector of control surface deflections, canard and tail
$\boldsymbol{\eta}$	=	augmented missile state vector
θ	=	pitch angle
λ	=	angle between the temporary and initial line of sight
μ	=	sliding mode control uncertainty controller parameter
σ	=	sliding variable
$\boldsymbol{\sigma}$	=	sliding vector
τ	=	time constant
Φ	=	transition matrix
ψ	=	function of individual contributions in computing the zero-effort miss
$\bar{(\cdot)}$	=	approximation/model

Subscripts

0	=	initial values
bf	=	body frame parallel to the inertial frame
br	=	body rotating frame
c	=	canard
E	=	evasive target
EN	=	evader component perpendicular to the line of sight
eq	=	equivalent control
I	=	inertial coordinate frame
kin	=	kinematics
M	=	missile
MN	=	missile component perpendicular to the line of sight
q	=	pitch rate
r	=	radial, along the line of sight
t	=	tail

Presented as Paper 6455 at the AIAA Guidance, Navigation, and Control Conference and Exhibit, San Francisco, California, 15–18 August 2005; received 4 May 2006; revision received 7 January 2007; accepted for publication 8 January 2007.

*Associate Professor, Department of Aerospace Engineering; moshe.idan@technion.ac.il. AIAA Associate Fellow.

†Senior Lecturer, Department of Aerospace Engineering; tal.shima@technion.ac.il. AIAA Senior Member.

‡Systems Engineer, Post Office Box 2250, Department M5; odedgol@rafael.co.il. AIAA Senior Member.

Z = zero-effort miss
α = angle of attack
δ_c = canard control
δ_t = tail control
λ = perpendicular to the line of sight

Superscripts

B = body contribution to the aerodynamics force and moment
c = command
max = maximum

I. Introduction

DESIGNING an interceptor missile involves tradeoffs between conflicting requirements. For example, to obtain the required agility in a high-end air-to-air interception engagement, a canard configuration is often employed due to its improved homing performance [1]; the canard fins, located in the front part of the fuselage, generate an aerodynamic force that is in the same direction as the required maneuvering force, thus generating (neglecting servo dynamics) an immediate response in the correct direction. However, if the missile is to perform sharp initial turns, canard control may limit its performance due to aerodynamic saturation at high angles of attack, and tail control may be preferred. By using both canard and tail controls, a favorable design compromise can be obtained to provide enhanced performance.

The additional degree of freedom offered by the dual-control system requires special consideration in the guidance and autopilot design. In many studies, the focus was on controlling the airframe. A sliding mode approach [2,3] with a linear strategy for blending the two control actions was suggested in several works [4–6]. Neural networks were used in [7] for the design of adaptive nonlinear control for an agile missile with forward and aft reaction control systems and aerodynamic tail control surfaces. In [8], the coefficient diagram method was used for an all aerodynamic tail fins and canard configuration. In recent papers [9–11], the focus was different; it was on designing the end-game guidance strategy for such a dual-control missile. The approach was based on the assumption that the additional degree of freedom can be best used by providing the guidance law with the capability of optimally imparting the commands to the two controls. In [9], the missile control limits were treated indirectly, by incorporating penalties on the use of the controls in the linear quadratic differential games formulation of the problem, whereas in [10], the control bounds were explicitly taken into account. The performance of these control schemes was investigated using high-order noisy simulation in [11] and the superiority over classical designs was advocated.

Integrated flight-control and guidance law design may enhance the end-game performance of the interceptor by accounting for the coupling between the control and guidance dynamics. Moreover, in a dual-control configuration it will inherently make use of the additional degree of freedom. In such designs, the entire guidance and control loop is stated as a solution to a finite horizon control problem, instead of the common approach treating the inner autopilot loop as an unrealistically infinite horizon one. The integrated design also allows for a more effective use of the information on the missile states in the guidance problem formulation, as opposed to using only the missile acceleration data in separated guidance loop designs. In [12], a game theoretic approach was used for the design of an integrated autopilot-guidance linear controller, which minimizes the final miss distance and control energy under worst case target maneuvers and measurements uncertainties. The feedback linearization method [13] was used in [14] in a finite horizon problem setting. In [15], a state-dependent Riccati differential equation approach was used for designing the integrated controller. Using a 6 degrees-of-freedom simulation, it was shown that the integrated controller provides improved miss distance statistics compared with the conventional two-loop design practice.

In recent papers [16,17], the sliding mode control (SMC) methodology was applied to the design of an integrated guidance-autopilot controller. The usefulness of SMC stems from being a nonlinear, robust control design approach enabling to maintain stability and performance in the presence of modeling errors. Simplified controllers are obtained using SMC by converting a tracking problem of an nth order dynamical system into a first-order stabilization problem. This approach leads to satisfactory performance in the presence of bounded but otherwise arbitrary parameter inaccuracies and model uncertainties. In [16], it was applied to obtain a two-loop design, using backstepping and high-order SMC methods. In the outer SMC-like guidance loop, a sliding surface that depends on the line-of-sight (LOS) rate was defined with the missile pitch rate used as a virtual control. The inner loop was designed to robustly enforce the pitch rate command of the outer loop in the presence of uncertainties. Numerical simulation was used to demonstrate the performance and robustness of the integrated design in tracking an evasive maneuvering target in the presence of atmospheric disturbances and uncertainty in the plant and actuator dynamics. In [17], SMC was used for the derivation of an integrated autopilot-guidance controller, using the zero-effort miss (ZEM) distance as its single sliding surface. The performance of the integrated controller was compared with that of two different two-loop designs and the superiority of the integrated design was demonstrated, especially in severe scenarios where spectral separation between guidance and flight control, implicitly assumed in any two-loop design, is not valid.

In the present paper, the SMC methodology is used for the design of an integrated guidance-autopilot controller for a missile controlled by two aerodynamic surfaces. Compared with the single control case, the additional degree of freedom allows for achieving other objectives in addition to guidance performance. One such objective may be improving the interceptor dynamic response. This may enhance guidance performance, but it may also be needed to address other considerations such as seeker or warhead working conditions. In the SMC context, this is obtained by introducing an additional sliding surface. This surface is selected using flight-control considerations, such as achieving improved stability and shaped/damped response.

In the next section, the actual, approximate, and linearized kinematics and dynamics models of the interception problem are introduced. Next, the integrated guidance-autopilot controller is synthesized, along with the definition of the two sliding surfaces used for the design. Then, the interaction between the surfaces and the homing performance is analyzed using nonlinear simulations. Concluding remarks are offered in the last section.

II. Model Derivation

A skid-to-turn cruciform, roll-stabilized missile with forward and aft maneuver surfaces is considered. The motion of such a missile can be separated into two perpendicular channels. Consequently, the guidance and control of a target interception problem can be treated as planar in each of these channels. We first present the full nonlinear kinematics and dynamics equations of the interception problem, which will serve for analysis. Then, approximate dynamics, which will be used for the design of the nonlinear sliding mode guidance-autopilot controller, are presented. Finally, linearized equations are derived, which will serve as the basis for the selection of the SMC sliding surfaces.

A. Nonlinear Kinematics and Dynamics

1. Engagement Kinematics

In Fig. 1, a schematic view of the planar end-game geometry is shown. Neglecting the gravitational force, the engagement kinematics, expressed in a polar coordinate system (r, λ) attached to the missile, is

$$\dot{r} = V_r \tag{1a}$$

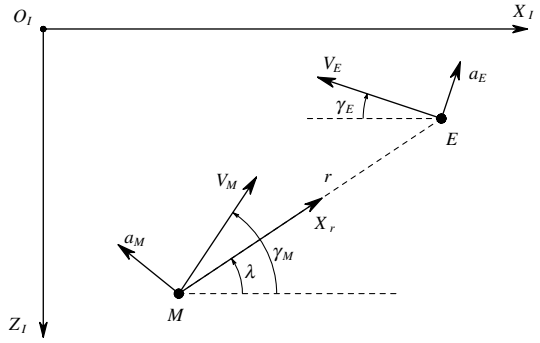

Fig. 1 Planar engagement geometry.

$$\dot{\lambda} = V_\lambda / r \tag{1b}$$

where the closing speed V_r is

$$V_r = -[V_M \cos(\gamma_M - \lambda) + V_E \cos(\gamma_E + \lambda)] \tag{2}$$

and the speed perpendicular to the LOS is

$$V_\lambda = -V_M \sin(\gamma_M - \lambda) + V_E \sin(\gamma_E + \lambda) \tag{3}$$

The interception duration or the time-to-go used in the subsequent derivations, is approximated by

$$t_{\text{go}} = -r/V_r, \qquad V_r < 0 \tag{4}$$

During the end game (the time of interest in our analysis), we assume that $V_r < 0$ and the engagement terminates when V_r crosses zero.

2. Target Dynamics

In this formulation, it is assumed that the evading target is moving at a constant speed and performs lateral maneuvers only. The lateral target dynamics are approximated by a first-order model

$$\dot{\gamma}_E = a_E / V_E \tag{5a}$$

$$\dot{a}_E = (a_E^c - a_E)/\tau_E \tag{5b}$$

where τ_E is the time constant of the target dynamics and a_E^c is the target maneuver command. We assume that $|a_E^c| \le a_E^{\max}$.

The target acceleration perpendicular to LOS, routinely used in guidance logic synthesis, is given by

$$a_{\text{EN}} = a_E \cos(\gamma_E + \lambda) \tag{6}$$

3. Missile Dynamics

The missile planar dynamics are expressed using the coordinate systems presented in Fig. 2. X_{bf}–M–Z_{bf} is parallel to the inertial frame X_I–O_I–Z_I, with its origin located at the missile's center of gravity (c.g.). It is used to express the missile attitude relative to the inertial frame. The missile equations of motion are derived in the rotating body fixed coordinate frame X_{br}–M–Z_{br}, where the X_{br} axis is aligned with the missile's longitudinal axis. It is assumed that

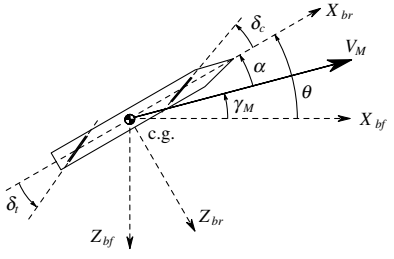

Fig. 2 Missile coordinate systems.

during the end game, the time of interest in our analysis, the missile speed is constant. Thus, the planar missile dynamics are given by

$$\dot{\alpha} = q - L(\alpha, \delta_c, \delta_t)/(mV_M) \tag{7a}$$

$$\dot{q} = M(\alpha, q, \delta_c, \delta_t)/I \tag{7b}$$

$$\dot{\theta} = q \tag{7c}$$

$$\dot{\delta}_c = \left(\delta_c^c - \delta_c\right)\Big/\tau_c \tag{7d}$$

$$\dot{\delta}_t = \left(\delta_t^c - \delta_t\right)\Big/\tau_t \tag{7e}$$

These surfaces are controlled by actuators, modeled by first-order dynamics with time constants τ_c and τ_t. The aerodynamic forces and moments are nonlinear, partly unknown functions of the related variables, in particular α, q, δ_c, and δ_t.

The missile flight path angle and acceleration perpendicular to the LOS are given by

$$\gamma_M = \theta - \alpha \tag{8}$$

$$a_{\text{MN}} = a_M \cos(\gamma_M - \lambda) \tag{9}$$

Here, the missile acceleration perpendicular to its velocity vector is given by

$$a_M = L(\alpha, \dot{\alpha}, q, \delta_c, \delta_t)/m \tag{10}$$

In modeling the missile dynamics, we assume that the lift and the aerodynamic pitch moment in Eqs. (7) are generated by the missile body and the control surfaces. This is modeled by

$$L/m = L_\alpha^B f_1(\alpha) + L_{\delta_c} f_2(\alpha + \delta_c) + L_{\delta_t} f_3(\alpha + \delta_t) \tag{11a}$$

$$M/I = M_\alpha^B f_4(\alpha) + M_q q + M_{\delta_c} f_5(\alpha + \delta_c) + M_{\delta_t} f_6(\alpha + \delta_t) \tag{11b}$$

where

$$L_\alpha^B = L_\alpha - L_{\delta_c} - L_{\delta_t} \tag{12a}$$

$$M_\alpha^B = M_\alpha - M_{\delta_c} - M_{\delta_t} \tag{12b}$$

$f_i(\cdot)$, $i = 1, \ldots, 6$ express the nonlinear aerodynamic characteristics of the missile.

B. Approximate Dynamics

We assume that the true dynamics of the target and missile are unknown to the designer of the missile autopilot and guidance. Thus, only approximate dynamics can be used, imposing modeling errors. These approximations are discussed next.

1. Target

The true target dynamics are assumed to be related to the approximate first-order linear model of Eq. (5b) by

$$\dot{a}_{\text{EN}} = (a_{\text{EN}}^c - a_{\text{EN}})/\tau_E + \Delta_{a\text{EN}} \tag{13}$$

where the target acceleration command and the modeling error are assumed to be bounded by

$$|a_{\text{EN}}^c| \le \bar{\Delta}_{a\text{EN}c} \tag{14a}$$

$$|\Delta_{a\mathrm{EN}}| \le \bar{\Delta}_{a\mathrm{EN}} \tag{14b}$$

2. Missile

The integrated controller, designed in the sequel, uses an approximation of the nonlinear model of Eqs. (7) and (11), i.e.,

$$\dot{\alpha} = q - [\bar{L}_{\alpha}^{B}\bar{f}_1(\alpha) + \bar{L}_{\delta_c}\bar{f}_2(\alpha+\delta_c) + \bar{L}_{\delta_t}\bar{f}_3(\alpha+\delta_t)]/V_M + \Delta_{\alpha} \tag{15a}$$

$$\dot{q} = \bar{M}_{\alpha}^{B}\bar{f}_4(\alpha) + \bar{M}_q q + \bar{M}_{\delta_c}\bar{f}_5(\alpha+\delta_c) + \bar{M}_{\delta_t}\bar{f}_6(\alpha+\delta_t) + \Delta_q \tag{15b}$$

$$\dot{\delta}_c = \left(\delta_c^c - \delta_c\right)\Big/\tau_c \tag{15c}$$

$$\dot{\delta}_t = \left(\delta_t^c - \delta_t\right)\Big/\tau_t \tag{15d}$$

where $\bar{L}_{(\cdot)}$, $\bar{M}_{(\cdot)}$, and $\bar{f}_i(\cdot)$, $i = 1,\ldots,6$ are approximations of their respective quantities and functions. Δ_{α} and Δ_q express the modeling errors, such as unmodeled nonlinearities and downwash effects, assumed to be bounded by

$$|\Delta_{\alpha}| \le \bar{\Delta}_{\alpha} \tag{16a}$$

$$|\Delta_q| \le \bar{\Delta}_q \tag{16b}$$

We assume no modeling errors on the actuators dynamics.

C. Linearized Kinematics and Dynamics

The definition of the sliding surfaces in the integrated guidance-autopilot design will be based on simplified kinematics and dynamics models. For these definitions it can be assumed that, during the end game, the missile and target deviations from the collision triangle are small. Thus, linearization of the end-game kinematics are performed around the initial LOS [18].

The linearized kinematics variables are depicted in Fig. 3, in which the X axis is aligned with the initial LOS. The approximate short-period linearized equations of motion are used for the missile dynamics [19].

The state vector of the integrated guidance-autopilot problem is defined by

$$\boldsymbol{x} = \begin{bmatrix} z & \dot{z} & a_{\mathrm{EN}} & \alpha & q & \delta_c & \delta_t \end{bmatrix}^T \tag{17}$$

Within the linear setting, a_{MN}, defined in Eq. (9), is approximated by

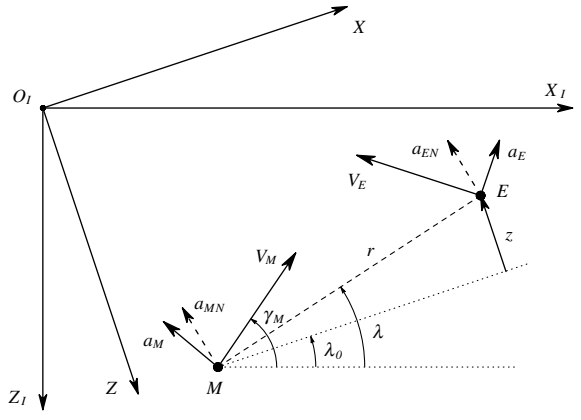

Fig. 3 Linearized end-game kinematics.

$$a_{\mathrm{MN}} \approx a_M \cos(\gamma_{M_0} - \lambda_0) \tag{18}$$

Thus, the missile acceleration normal to the initial LOS is given by

$$a_{\mathrm{MN}} = C_M\begin{bmatrix} \alpha & q & \delta_c & \delta_t \end{bmatrix}^T \tag{19}$$

where

$$C_M = \begin{bmatrix} L_{\alpha} & 0 & L_{\delta_c} & L_{\delta_t} \end{bmatrix}\cos(\gamma_{M_0} - \lambda_0) \tag{20}$$

The equations of motion of the integrated dynamics are

$$\dot{\boldsymbol{x}} = A\boldsymbol{x} + B\boldsymbol{\delta}^c + Ga_{\mathrm{EN}}^c \tag{21}$$

where

$$A = \begin{bmatrix} A_{\mathrm{kin}} & A_{12} \\ [0]_{4\times 3} & A_M \end{bmatrix}, \qquad A_{12} = \begin{bmatrix} [0]_{1\times 4} \\ -C_M \\ [0]_{1\times 4} \end{bmatrix}, \qquad B = \begin{bmatrix} [0]_{3\times 2} \\ B_M \end{bmatrix} \tag{22}$$

$$G = \begin{bmatrix} 0 & 0 & 1/\tau_E & 0 & 0 & 0 & 0 \end{bmatrix}^T \tag{23}$$

and $[0]_{a\times b}$ denotes a matrix of zeros with appropriate dimensions. From the equations of relative motion normal to the initial LOS

$$A_{\mathrm{kin}} = \begin{bmatrix} 0 & 1 & 0 \\ 0 & 0 & 1 \\ 0 & 0 & -1/\tau_E \end{bmatrix} \tag{24}$$

Using Eqs. (7) and (11), the linearized short-period dynamics, coupled with the first-order control surface actuation models of Eqs. (7d) and (7e), yield

$$A_M = \begin{bmatrix} -L_{\alpha}/V_M & 1 & -L_{\delta_c}/V_M & -L_{\delta_t}/V_M \\ M_{\alpha} & M_q & M_{\delta_c} & M_{\delta_t} \\ 0 & 0 & -1/\tau_c & 0 \\ 0 & 0 & 0 & -1/\tau_t \end{bmatrix}$$
$$B_M = \begin{bmatrix} 0 & 0 \\ 0 & 0 \\ 1/\tau_c & 0 \\ 0 & 1/\tau_t \end{bmatrix} \tag{25}$$

III. Integrated Sliding Mode Control Guidance: Autopilot Synthesis

The SMC design methodology entails three major steps: 1) selection of a sliding manifold $\boldsymbol{\sigma} = 0$ to ensure stable desired dynamic characteristics of the system once in the sliding mode; 2) computation of the equivalent control to impose $\dot{\boldsymbol{\sigma}} = 0$ once on the sliding surfaces, while using an approximate model of the system dynamics; and 3) choosing an uncertainty controller to ensure stability and finite time convergence to the surfaces when $\boldsymbol{\sigma} \neq 0$.

The definition of the sliding surfaces will be based on the linearized models presented in Sec. II.C. The equivalent and uncertainty controllers will be designed using the full nonlinear kinematics and dynamics models of the problem presented in Secs. II.A and II.B, respectively.

A. Sliding Surfaces

The concept of ZEM [18] is very useful for deriving and understanding missile guidance laws, especially those obtained using optimal control and differential games theories. In a one-sided, optimal-control, optimization problem it has the physical meaning of being the miss distance if, from the current time onward, the interceptor does not apply controls and the target performs the expected maneuver. In a two-sided differential game problem, ZEM is the miss distance if, from the current time onward, both players do not apply controls. Commonly, it is the expected miss distance

computed using the homogenous solution of the associated linearized engagement equations of motion. Its usefulness in missile guidance problems, where the only state of importance is the miss distance, stems from reducing the n-dimensional guidance problem to a scalar one. Moreover, its linear dynamics equation depends only on the system inputs. The ZEM depends on the problem formulation and model.

In a recent study [17], for a canard controlled missile (single-input/single-output problem), the differential game-based ZEM was chosen as the single sliding surface for an integrated guidance-autopilot design. This choice does not require any assumption regarding the future maneuvers of the target. If the system response is maintained on this surface, it provides zero miss distance. Moreover, once on the surface, no control action is needed to ensure interception in the nominal linear case with perfect modeling and no target maneuvers. In a realistic nonlinear environment, with modeling errors and target maneuvers, the uncertainty control element of the SMC solution is designed to nullify deviations from the sliding surface in finite time.

The governing equation that is used to define the ZEM is the linearized Eq. (21). Because of the definition of ZEM, assuming that

$$\boldsymbol{\delta}^{c} = [\,\delta_c^c \quad \delta_t^c\,]^T$$

and a_{EN}^c are identically zero, the measurementlike equation of ZEM denoted by Z is

$$Z = C_Z \boldsymbol{x}(t_{\mathrm{go}}) \tag{26}$$

where

$$C_Z = \begin{bmatrix} 1 & 0 & 0 & 0 & 0 & 0 & 0 \end{bmatrix} \tag{27}$$

To compute $\boldsymbol{x}(t_{\mathrm{go}})$, we introduce the transition matrix $\Phi(t_f, t)$, which, for the linear time-invariant system of Eq. (21), is given by

$$\Phi(t_f, t) = \Phi(t_{\mathrm{go}}) = \exp(A t_{\mathrm{go}}) \tag{28}$$

Thus,

$$\boldsymbol{x}\,(t_{\mathrm{go}}) = \Phi(t_{\mathrm{go}})\boldsymbol{x} \tag{29}$$

Using the expressions of Eqs. (28) and (29) in Eq. (26), the ZEM is expressed as

$$\begin{aligned} Z \triangleq C_Z \Phi(t_{\mathrm{go}})\boldsymbol{x} = z + \dot{z} t_{\mathrm{go}} + a_{\mathrm{EN}} \tau_E^2 \psi(t_{\mathrm{go}}/\tau_E) + \psi_\alpha(t_{\mathrm{go}})\alpha \\ + \psi_q(t_{\mathrm{go}})q + \psi_{\delta_c}(t_{\mathrm{go}})\delta_c + \psi_{\delta_t}(t_{\mathrm{go}})\delta_t \end{aligned} \tag{30}$$

where

$$\psi(\zeta) = \exp(-\zeta) + \zeta - 1 \tag{31}$$

and $\psi_\alpha(t_{\mathrm{go}})$, $\psi_q(t_{\mathrm{go}})$, $\psi_{\delta_c}(t_{\mathrm{go}})$, and $\psi_{\delta_t}(t_{\mathrm{go}})$ are complicated functions of the system parameters and t_{go}, and hence of the kinematics variables.

Assuming small deviations from a collision triangle, the displacement z normal to the initial LOS can be approximated by $z \approx (\lambda - \lambda_0) r$. Differentiating with respect to time yields

$$z + \dot{z} t_{\mathrm{go}} = -V_r t_{\mathrm{go}}^2 \dot{\lambda} = V_\lambda t_{\mathrm{go}} \tag{32}$$

Thus, the first two terms in Eq. (30) can be expressed as a function of the kinematics variables V_r, V_λ, and r. The last four complicated terms of Eq. (30) can be obtained from the numerically computed transition matrix $\Phi(t_{\mathrm{go}})$ associated with A of Eq. (22). Using this, together with the relationship obtained in Eq. (32), the ZEM of Eq. (30) is expressed as

$$Z = V_\lambda t_{\mathrm{go}} + a_{\mathrm{EN}} \tau_E^2 \psi(t_{\mathrm{go}}/\tau_E) + C_Z \Phi(t_{\mathrm{go}})\boldsymbol{\eta} \tag{33}$$

where

$$\boldsymbol{\eta} = \begin{bmatrix} 0 & 0 & 0 & \alpha & q & \delta_c & \delta_t \end{bmatrix}^T \tag{34}$$

contains the missile variables of the state vector preceded by zeros.

In the current two-input, multi-input/multi-output problem we seek an additional sliding surface to take advantage of the design degrees of freedom offered by the dual-control configuration. The sought-after surface should not interfere with the first surface, ensuring zero miss distance if the system is kept on it. Moreover, if possible, it should not restrict the canard control, as it has been shown in several studies that it has a higher effect in enhancing the homing performance [1,11,20]. Thus, we choose the following sliding surface based on flight-control considerations, without explicitly referring to the canard control

$$\sigma_M = \bar{M}_\alpha^B \bar{f}_4(\alpha) + \bar{M}_{\delta_t} \bar{f}_6(\alpha + \delta_t) \tag{35}$$

The preceding equation expresses the angle of attack and tail contributions to the missile aerodynamic pitch moments, resulting from the approximate model of Eq. (15b). Because the missile is assumed stable, this surface enforces the tail control to produce a moment equal to the one generated by the body, but in an opposite direction. Thus, missile response is damped, and trim is enforced provided there are no maneuver commands issued by the canard. The canard commands may be caused by guidance considerations to remain on the $Z = 0$ surface.

In the sequel, the two sliding surfaces are grouped into the sliding vector

$$\boldsymbol{\sigma} = [\,Z \quad \sigma_M\,]^T$$

B. Equivalent Controller

The equivalent controller is designed to maintain the system on the sliding surfaces, once those are attained. This is obtained by imposing $\dot{\boldsymbol{\sigma}} = 0$. Thus, the derivation of the equivalent controller will require a derivative of the sliding vector.

The time derivative of ZEM is given by

$$\begin{aligned} \dot{Z} = \dot{V}_\lambda t_{\mathrm{go}} + V_\lambda \dot{t}_{\mathrm{go}} + \tau_E^2 [\dot{a}_{\mathrm{EN}} \psi(t_{\mathrm{go}}/\tau_E) + a_{\mathrm{EN}} \psi'(t_{\mathrm{go}}/\tau_E)\dot{t}_{\mathrm{go}}] \\ + C_Z [\Phi'(t_{\mathrm{go}})\dot{t}_{\mathrm{go}}\boldsymbol{\eta} + \Phi(t_{\mathrm{go}})\dot{\boldsymbol{\eta}}] \end{aligned} \tag{36}$$

where

$$\dot{V}_r = V_\lambda^2/r + a_M \sin(\gamma_M - \lambda) + a_E \sin(\gamma_E + \lambda) \tag{37}$$

$$\dot{V}_\lambda = -V_\lambda V_r/r - a_M \cos(\gamma_M - \lambda) + a_E \cos(\gamma_E + \lambda) \tag{38}$$

$$\dot{t}_{\mathrm{go}} = -1 + \dot{V}_r r/V_r^2 \tag{39}$$

and

$$\psi'(t_{\mathrm{go}}/\tau_E) = \partial\psi(t_{\mathrm{go}}/\tau_E)/\partial t_{\mathrm{go}} = [t_{\mathrm{go}}/\tau_E - \psi(t_{\mathrm{go}}/\tau_E)]/\tau_E \tag{40}$$

$$\Phi'(t_{\mathrm{go}}) = \partial\Phi(t_{\mathrm{go}})/\partial t_{\mathrm{go}} = \Phi(t_{\mathrm{go}})A \tag{41}$$

Because of the structure of $\boldsymbol{\eta}$, its derivative $\dot{\boldsymbol{\eta}}$ used in Eq. (36) is given by Eqs. (15), preceded by three zero elements. This can be expressed by

$$\dot{\boldsymbol{\eta}} = \boldsymbol{f}(\boldsymbol{\eta}) + \Delta\boldsymbol{f}(\boldsymbol{\eta}) + B\boldsymbol{\delta}^c \tag{42}$$

where $\boldsymbol{f}(\boldsymbol{\eta})$ are the known state dependent terms of Eqs. (15), whereas $\Delta\boldsymbol{f}(\boldsymbol{\eta})$ contains the modeling errors Δ_α and Δ_q in its fourth and fifth elements, respectively. The matrix B is defined in Eq. (22).

The time derivative of the second surface is given by

$$\dot{\sigma}_M = \left[\bar{M}_\alpha^B \bar{f}_4'(\alpha)\right]\dot{\alpha} + \left[\bar{M}_{\delta_t} \bar{f}_6'(\alpha + \delta_t)\right](\dot{\alpha} + \dot{\delta}_t) \tag{43}$$

where $\bar{f}_i'(\cdot)$, $i = 4, 6$ denote the partial derivatives of the functions $\bar{f}_i(\cdot)$, $i = 4, 6$ with respect to their respective arguments. In this equation, $\dot{\alpha}$ is computed using Eq. (15a) or, equivalently, equals the fourth element of $\boldsymbol{f}(\boldsymbol{\eta}) + \Delta\boldsymbol{f}(\boldsymbol{\eta})$ in Eq. (42), i.e.,

$$\dot{\alpha} = C_\alpha \boldsymbol{f}(\boldsymbol{\eta}) + \Delta_\alpha \tag{44}$$

where

$$C_\alpha = [0 \quad 0 \quad 0 \quad 1 \quad 0 \quad 0 \quad 0]$$

The relations of Eqs. (13), (15d), (42), and (44) are used in Eqs. (36) and (43) to yield

$$\dot{\boldsymbol{\sigma}} = \boldsymbol{g} + \Delta\boldsymbol{g} + H\boldsymbol{\delta}^c \tag{45}$$

where

$$\boldsymbol{g} = \begin{Bmatrix} \dot{V}_\lambda t_{\text{go}} + V_\lambda \dot{t}_{\text{go}} + a_{\text{EN}}\tau_E^2[\psi'(t_{\text{go}}/\tau_E)\dot{t}_{\text{go}} - \psi(t_{\text{go}}/\tau_E)/\tau_E] \\ [\bar{M}_\alpha^B \bar{f}_4'(\alpha) + \bar{M}_{\delta_t}\bar{f}_6'(\alpha+\delta_t)]C_\alpha \boldsymbol{f}(\boldsymbol{\eta}) - [\bar{M}_{\delta_t}\bar{f}_6'(\alpha+\delta_t)]\delta_t/\tau_t \end{Bmatrix} + \begin{Bmatrix} C_Z\Phi(t_{\text{go}})[A\dot{t}_{\text{go}}\boldsymbol{\eta} + \boldsymbol{f}(\boldsymbol{\eta})] \\ 0 \end{Bmatrix} \tag{46a}$$

$$\Delta\boldsymbol{g} = \begin{Bmatrix} (a_{\text{EN}}^c + \tau_E\Delta_{a_{\text{EN}}})\tau_E\psi(t_{\text{go}}/\tau_E) + C_Z\Phi(t_{\text{go}})\Delta\boldsymbol{f}(\boldsymbol{\eta}) \\ [\bar{M}_\alpha^B\bar{f}_4'(\alpha) + \bar{M}_{\delta_t}\bar{f}_6'(\alpha+\delta_t)]\Delta_\alpha \end{Bmatrix} \tag{46b}$$

$$H = \begin{bmatrix} C_Z\Phi(t_{\text{go}})B \\ [0 \quad \bar{M}_{\delta_t}\bar{f}_6'(\alpha+\delta_t)/\tau_t] \end{bmatrix} \tag{46c}$$

The particular choice of the sliding surfaces ensures that the matrix H in Eq. (46c) is upper triangular with nonzero terms on the diagonal, and hence nonsingular. Using the bounds in Eqs. (14) and (16), the two elements of $\Delta\boldsymbol{g}$ can be bounded as

$$|\Delta g_i| \le \bar{\Delta}_{g_i}, \qquad i = 1, 2 \tag{47}$$

In the absence of modeling errors and target maneuvers, once the system reaches the sliding surface it will remain on it using the equivalent control command $\boldsymbol{\delta}_{\text{eq}}^c$ given by

$$\boldsymbol{\delta}_{\text{eq}}^{\,c} = -H^{-1}\boldsymbol{g} \tag{48}$$

C. Uncertainty Controller

Modeling uncertainties and disturbances may cause the system to depart from the sliding surfaces. To accommodate these departures, the equivalent controller is augmented by a second component, sometimes referred to as the *uncertainty controller*. The goal of this uncertainty controller is to drive the system to the sliding surface in finite time, while ensuring closed-loop stability. The design of the uncertainty controller is based on the approximate models of the system dynamics given in Eqs. (13–16). The kinematics model of Eqs. (1–3) is assumed to be known exactly.

The integrated guidance-control logic is designed using the Lyapunov function candidate

$$\mathcal{L} = \tfrac{1}{2}\boldsymbol{\sigma}^T\boldsymbol{\sigma} \tag{49}$$

The time derivative of this Lyapunov function candidate is given by

$$\dot{\mathcal{L}} = \boldsymbol{\sigma}^T\dot{\boldsymbol{\sigma}} = \boldsymbol{\sigma}^T(\boldsymbol{g} + \Delta\boldsymbol{g} + H\boldsymbol{\delta}^c) \tag{50}$$

where the result in Eq. (45) was used for $\dot{\boldsymbol{\sigma}}$. The SMC controller is chosen to be

$$\boldsymbol{\delta}^{\,c} = \boldsymbol{\delta}_{\text{eq}}^c - H^{-1}\mathcal{M}\text{sgn}(\boldsymbol{\sigma}) \tag{51}$$

The second term on the right-hand side of Eq. (51) is the uncertainty controller, where $\mathcal{M} = \text{diag}(\mu_1, \mu_2)$ is a diagonal 2×2 matrix, and

$$\text{sgn}\,(\boldsymbol{\sigma}) = [\,\text{sgn}(\sigma_1) \quad \text{sgn}(\sigma_2)\,]^T$$

With this controller, the derivative of the Lyapunov function candidate becomes

$$\dot{\mathcal{L}} = \boldsymbol{\sigma}^T[\Delta\boldsymbol{g} - \mathcal{M}\text{sgn}(\boldsymbol{\sigma})] = \sum_{i=1}^{2}\sigma_i[\Delta g_i - \mu_i\text{sgn}(\sigma_i)] \tag{52}$$

Using the bounds in Eqs. (47), this derivative can be bounded by

$$\dot{\mathcal{L}} \le -\sum_{i=1}^{2}|\sigma_i|(\mu_i - \bar{\Delta}_{g_i}) \tag{53}$$

Choosing

$$\mu_i > \bar{\Delta}_{g_i}, \qquad i = 1, 2 \tag{54}$$

will guaranty a negative definite Lyapunov function derivative and hence convergence to the two-dimensional sliding manifold in finite time. Moreover, the values of μ_i, $i = 1, 2$ could be tuned to emphasize the attraction of one sliding surface compared with the other. In a realistically noisy and uncertain interception environment, a boundary layer around the sliding surface can be employed to provide smooth control commands and to avoid chattering caused by the sgn function in Eq. (51).

IV. Performance Analysis

Performance of the proposed integrated guidance and control algorithm is evaluated through numerical simulations, incorporating the nonlinear models of Eqs. (1), (5), and (7). A sample run is first examined, followed by a Monte Carlo study.

A. Scenario

The numerical study was performed for a generic interceptor model, which is based on the missile control example introduced in [21] and used in [11]. It is assumed that the target performs a square-wave evasive maneuver with a period of ΔT and a phase of $\Delta\phi$ relative to the beginning of the simulation. The initial missile-target range was set to 1000 m. The initial missile velocity vector was aligned with the initial LOS. The target initial velocity vector is pointed 20 deg away from the initial LOS. An example of the engagement geometry and trajectories is plotted in Fig. 4.

The missile and target model parameters are given in Table 1. The functions $f_i(\cdot)$, $i = 1, \ldots, 6$ were chosen to be the standard saturation functions

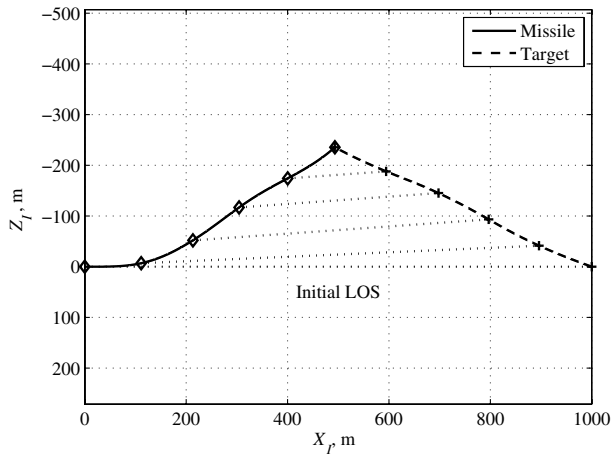

Fig. 4 Sample run engagement trajectories.

Table 1 Simulation parameters

Missile		Target
Actual	Model	
$V_M = 380$ m/s	$\bar{L}_\alpha^B = 1190$ m/s^2	$V_E = 380$ m/s
$\tau_c = 0.02$ s	$\bar{L}_{\delta_c} = 40$ m/s^2	$a_E^{\max} = 15$ g
$\tau_t = 0.02$ s	$\bar{L}_{\delta_t} = 40$ m/s^2	$\Delta T = 1$ s
	$\bar{M}_\alpha^B = -100$ s^{-2}	$\Delta\phi[0, 1]$ s
	$\bar{M}_q = -5$ s^{-1}	$\tau_E[0.05, 0.2]$ s
	$\bar{M}_{\delta_c} = 80$ s^{-2}	
	$\bar{M}_{\delta_t} = -80$ s^{-2}	

$$\text{sat}(u) = \begin{cases} U_m & u > U_m \\ u & |u| \le U_m \\ -U_m & u < -U_m \end{cases} \tag{55}$$

with $U_m = 25$ deg for all i. Moreover, the fins' deflections were limited to ± 25 deg. For the controller design, the model functions $\bar{f}_4(\cdot)$ and $\bar{f}_6(\cdot)$, which have to be differentiated with respect to their argument [see Eq. (43)], were chosen as smooth approximations of Eq. (55).

B. Sample Run Performance

The performance of the proposed guidance and control design is first evaluated for a sample run. The target maneuver was characterized by $\tau_E = 0.1$ s and $\Delta\phi = 0$ s. In Fig. 5, the ZEM and σ_M, computed using Eqs. (33) and (35), respectively, are shown. The missile and target accelerations are given in Fig. 6, and the canard and tail deflection angles are plotted in Fig. 7. The initial ZEM error, caused by the heading error, is decreased and maintained close to the desired surface, i.e., $Z = 0$, up to interception. Deviations from the second surface occur as a result of tail saturation, evident in Fig. 7. This happens when high accelerations are generated (see Fig. 6) to close the initial heading error and account for the target evasive maneuvers. When the tail is not saturated, the sliding variable remains close to zero, e.g., in the time interval of 1.05–1.25 s. The ZEM surface is maintained mainly due to the effect of the canard control. This is possible because the second surface (σ_M) does not explicitly restrict the canard control. Note that strong activity of the canard control is required to achieve this goal.

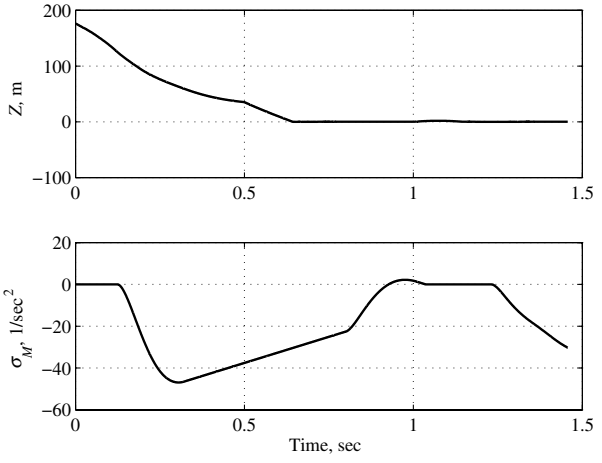

Fig. 5 ZEM and σ_M for a sample run.

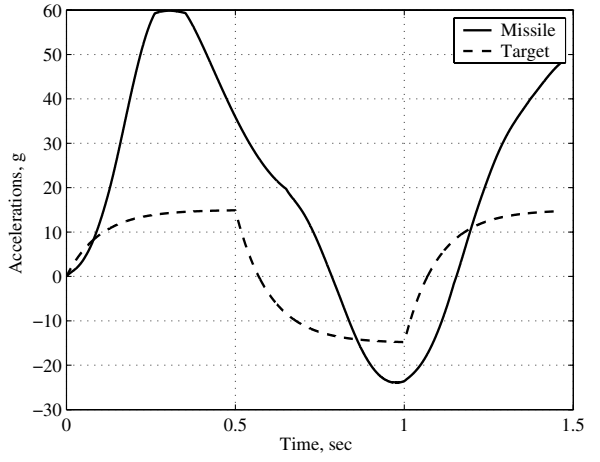

Fig. 6 Missile and target acceleration profiles for a sample run.

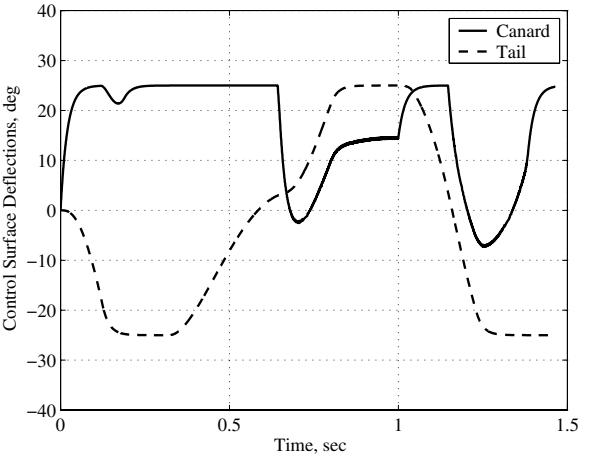

Fig. 7 Canard and tail deflections for a sample run.

C. Homing Performance

The homing performance of the proposed algorithm is evaluated by a Monte Carlo simulation study consisting of 100 sample runs for each test point. In these simulations, for each test case, the random variables were chosen as the maneuver phase $\Delta\phi$ of the target and the missile aerodynamic parameters (L_α^B, L_{δ_c}, L_{δ_t}, M_α^B, M_q, M_{δ_c}, and M_{δ_t}). We assume these parameters to be distributed uniformly, where $\Delta\phi \sim U(-.5, .5)$ s and the aerodynamics coefficients of the missile varied randomly by $\pm 10\%$ around the model values given in Table 1. Results are presented for targets with different dynamics characteristics, specified by the time constant τ_E. Although an entire range of τ_E values was tested (see Table 1), for brevity only two representative cases are shown, depicting the effect of target maneuverability on the interception accuracy.

The cumulative distribution of the miss distance for the nominal missile parameters (i.e., no uncertainty in the missile aerodynamic data) is plotted in Figs. 8 and 9 for $\tau_E = 0.1$ s and $\tau_E = 0.15$ s, respectively. The plots show the results for various values of μ_2, the

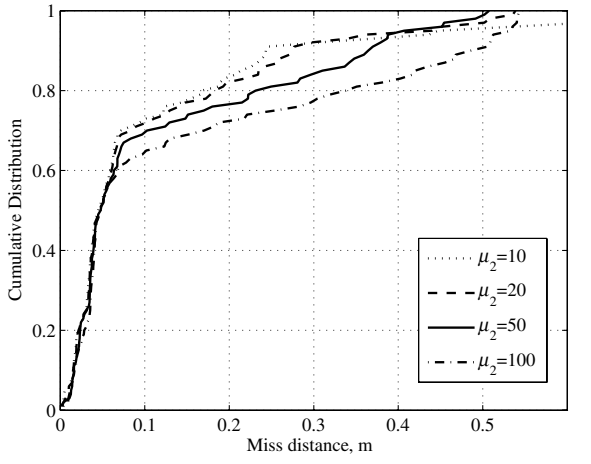

Fig. 8 Homing performance for the nominal parameters; $\tau_E = 0.1$ s.

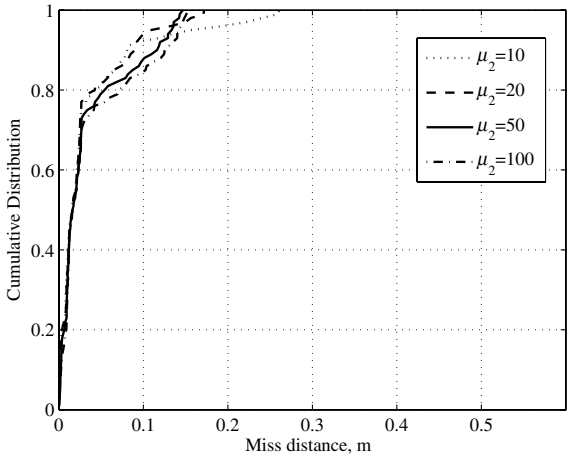

Fig. 9 Homing performance for the nominal parameters; $\tau_E = 0.15$ s.

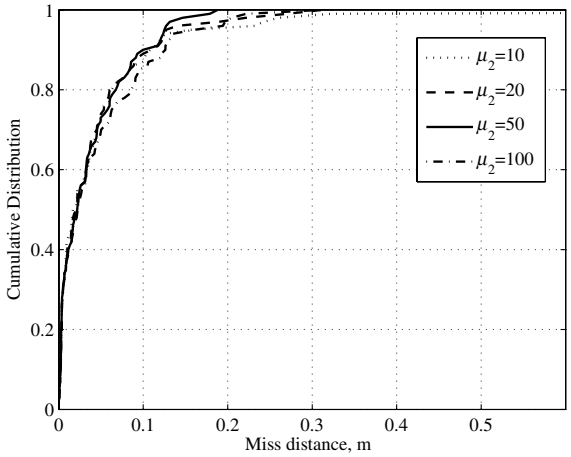

Fig. 11 Homing performance for 10% uncertainty in the aerodynamic parameters; $\tau_E = 0.15$ s.

gain of the uncertainty controller of the flight-control motivated sliding surface. The results reveal that for approximately 50% of the cases for targets with a higher bandwidth (Fig. 8) and for approximately 80% for the "slower" targets (Fig. 9) the miss distance is negligible (less than 5 cm).

The effect of changing the value of the gain μ_2 is noticeable only for the larger miss distances. For example, for $\tau_E = 0.1$ s (Fig. 8) and a gain of $\mu_2 = 10$, approximately 90% of the runs end with miss distances that are lower than 0.25 m. Viewed from a different perspective, using a kill mechanism with a lethal radius of 0.25 m will provide a single-shot kill probability of 90%. In comparison, for $\mu_2 = 100$ the same kill probability can be obtained only with a lethal radius of 0.5 m. From both figures it is apparent that changing the performance requirement, for example from 90% kill probability to 99%, may require a different choice of the gain μ_2. Also, from comparing both figures it is clear that, as expected, as τ_E increases the homing performance improves, i.e., to achieve the same single-shot kill probability a smaller lethal radius is required.

In Figs. 10 and 11, the cumulative distribution of the miss distance is plotted for 10% uncertainty in the missile parameters. The plots show the results for various values of μ_2. Figure 10 is obtained for $\tau_E = 0.1$ s and Fig. 11 for $\tau_E = 0.15$ s. The same qualitative results discussed before for the nominal missile parameters are repeated here for the case with uncertainties. By comparison to Figs. 8 and 9, it is evident that the homing performance somewhat degrades with the introduction of uncertainties. For example, for a target with a time constant $\tau_E = 0.15$ s and when there is no uncertainty in the missile parameters, 90% of the miss distances are lower than 8 cm, attained when selecting $\mu_2 = 10$ (see Fig. 9). In the same case with uncertainty, 90% of the miss distances are lower than 10 cm when selecting $\mu_2 = 50$ (see Fig. 11).

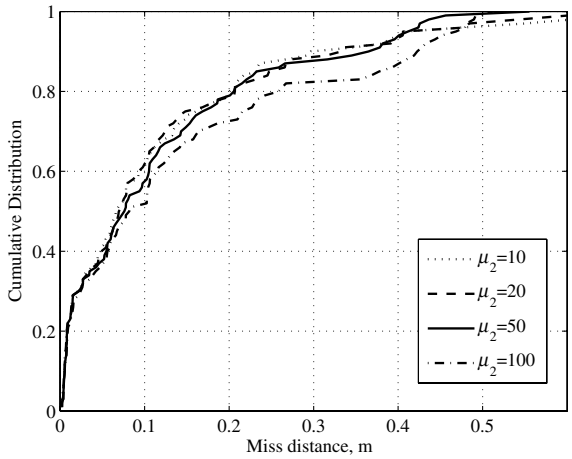

Fig. 10 Homing performance for 10% uncertainty in the aerodynamic parameters; $\tau_E = 0.1$ s.

From Figs. 8–11 it is apparent that increasing μ_2 up to a certain level improves the missile dynamic characteristics and consequently the interception accuracy. However, using a very high gain may result in degraded homing performance, observed, for example, in the $\mu_2 = 100$ case for the parameters of Fig. 8. This can be attributed to the fact that an increased emphasis on the flight-control motivated sliding variable implies a reduced emphasis on the guidance motivated ZEM sliding variable Z. For the current example, a good selection of the gain for the second surface is $\mu_2 = 50$, with a relative small sensitivity of the performance around that value.

V. Conclusions

An integrated guidance-autopilot design approach for an interceptor with forward and aft control mechanisms was presented in this paper. In contrast to the conventional two-loop design, it was shown that the integrated controller can account simultaneously for the guidance and autopilot requirements by using the additional degree of freedom offered by the dual-control configuration.

The integrated design, carried out using the sliding mode approach, required the definition of two sliding surfaces. Motivated by the recent results of a single controller integrated guidance-control design, one surface was defined as the zero-effort miss distance, encountered in the differential game formulation of the interception problem. Because, compared with tail control, canard control is more effective in enhancing the homing performance, an autopilot oriented sliding variable that does not restrict the canard control was introduced to define the second sliding surface. Monte Carlo analysis was used to investigate the interaction between the two sliding variables. The results show that remaining on both guidance and autopilot oriented sliding surfaces is important to achieve good homing performance, whereas emphasizing one surface over the other may result in degraded performance.

Robustness to target maneuvering and interceptor parameters uncertainties was shown. The results indicate that using the derived guidance law, small miss distances can be obtained even in stringent interception scenarios and in the presence of modeling errors.

References

[1] Gutman, S., "Superiority of Canards in Homing Missiles," *IEEE Transactions on Aerospace and Electronic Systems*, Vol. 39, No. 3, 2003, pp. 740–746.

[2] Utkin, V. I., *Sliding Modes in Control and Optimization*, Springer–Verlag, Berlin, 1992.

[3] Slotine, J. J. E., and Li, W., *Applied Nonlinear Control*, Prentice–Hall, Upper Saddle River, NJ, 1991, Chap. 7, pp. 276–307.

[4] Bhat, M. S., Bai, D. S., Powly, A. A., Swami, K. N., and Ghose, D., "Variable Structure Controller Design with Application to Missile Tracking," *Journal of Guidance, Control, and Dynamics*, Vol. 24, No. 4, 2001, pp. 859–862.

[5] Thukral, A., and Innocenti, M., "Sliding Mode Missile Pitch Autopilot

Synthesis for High Angle of Attack Maneuvering," *IEEE Transactions on Control Systems Technology*, Vol. 6, No. 3, 1998, pp. 359–371.

[6] Weil, R. D., and Wise, K. A., "Blended Aero and Reaction Jet Missile Autopilot Design Using VSS Techniques," *Proceedings of the 30th IEEE Conference on Decision and Control*, IEEE Publications, Piscataway, NJ, 1991, pp. 2828–2829.

[7] Menon, P. K., and Iragavarapu, V. R., "Adaptive Techniques for Multiple Actuator Blending," *Proceedings of the AIAA Guidance, Navigation, and Control Conference*, CP-4494, AIAA, Washington, D.C., 1998.

[8] Manabe, S., "Application of Coefficient Diagram Method to Dual-Control-Surface Missile," *Proceedings of the 15th IFAC Symposium on Automatic Control in Aerospace*, Elsevier Science & Technology, Oxford, England, U.K., 2001, pp. 441–446.

[9] Shima, T., and Golan, O. M., "Linear Quadratic Differential Games Guidance Laws for Dual Controlled Missiles," *IEEE Transactions on Aerospace and Electronic Systems* (to be published), 2007.

[10] Shima, T., and Golan, O. M., "Bounded Differential Games Guidance Law for Dual-Controlled Missiles," *IEEE Transactions on Control Systems Technology*, Vol. 14, No. 4, 2006, pp. 719–724.

[11] Shima, T., and Golan, O. M., "End-Game Guidance Laws for Dual Control Missiles," *Journal of Aerospace Engineering*, Vol. 219, No. 2, 2005, pp. 157–170.

[12] Lin, C. F., Wang, Q., Speyer, J. L., Evers, J. H., and Cloutier, J. R., "Integrated Estimation, Guidance, and Control System Design using Game Theoretic Approach," *Proceedings of the American Control Conference*, American Automatic Control Council, Evanston, IL, 1992, pp. 3220–3224.

[13] Khalil, H. K., *Nonlinear Systems*, 3rd ed., Prentice–Hall, Upper Saddle River, NJ, 2002, Chap. 13.

[14] Menon, P. K., Sweriduk, G. D., and Ohlmeyer, E. J., "Optimal Fixed-Interval Integrated Guidance-Control Laws for Hit-to-Kill Missiles," *Proceeding of the AIAA Guidance, Navigation, and Control Conference*, CP-5579, AIAA, Washington, D.C., 2003.

[15] Palumbo, N. F., and Jackson, T. D., "Integrated Missile Guidance and Control: a State Dependent Riccati Differential Equation Approach," *Proceedings of the IEEE International Conference on Control Applications*, IEEE Publications, Piscataway, NJ, 1999, pp. 243–248.

[16] Shkolnikov, I., Shtessel, Y. B., and Lianos, D., "Integrated Guidance-Control System of a Homing Interceptor: Sliding Mode Approach," *Proceeding of the AIAA Guidance, Navigation, and Control Conference*, CP-4218, AIAA, Washington, D.C., 2001.

[17] Shima, T., Idan, M., and Golan, O. M., "Sliding-Mode Control for Integrated Missile Autopilot Guidance," *AIAA Journal*, Vol. 29, No. 2, 2006, pp. 250–260.

[18] Zarchan, P., *Tactical and Strategic Missile Guidance*, Progress in Astronautics and Aeronautics, Vol. 176, AIAA, Washington, D.C., 1997, pp. 20–28.

[19] Blakelock, J. H., *Automatic Control of Aircraft and Missiles*, 2nd ed., Wiley, New York, 1991, Chap. 7.

[20] Shima, T., "Capture Conditions in a Pursuit-Evasion Game Between Players with Biproper Dynamics," *Journal of Optimization Theory and Application*, Vol. 126, No. 3, 2005, pp. 503–528.

[21] Friedland, B., *Control System Design: an Introduction to State Space Methods*, McGraw–Hill, New York, 1986, pp. 247–248.